Airborne L-Band Radio Frequency Interference Observations From the SMAPVEX08 Campaign and Associated Flights

James Park, *Student Member, IEEE*, J. T. Johnson, *Fellow, IEEE*, Ninoslav Majurec, Noppasin Niamsuwan, *Member, IEEE*, Jeffrey R. Piepmeier, *Member, IEEE*, Priscilla N. Mohammed, *Member, IEEE*, Christopher S. Ruf, *Fellow, IEEE*, Sidharth Misra, Simon H. Yueh, *Fellow, IEEE*, and Steve J. Dinardo, *Member, IEEE*

***Abstract*—Statistics of radio frequency interference (RFI) observed in the band 1398–1422 MHz during an airborne campaign in the United States are reported for use in analysis and forecasting of L-band RFI for microwave radiometry. The observations were conducted from September to October 2008, and included approximately 92 h of flight time, of which approximately 20 h of "transit" or dedicated RFI observing flights are used in compiling the statistics presented. The observations used include outbound and return flights from Colorado to Maryland, as well as RFI surveys over large cities. The Passive Active L-Band Sensor (PALS) radiometer of NASA Jet Propulsion Laboratory augmented by three dedicated RFI observing systems was used in these observations. The complete system as well as the associated RFI characterization approaches are described, along with the resulting RFI statistical information and examinations of specific RFI sources. The results show that RFI in the protected L-band spectrum is common over North America, although the resulting interference when extrapolated to satellite observations will appear as "low-level" corruption that will be difficult to detect for traditional radiometer systems.**

***Index Terms*—Microwave radiometry, radio frequency interference.**

I. Introduction

THE CORRUPTION of microwave radiometer observations by radio frequency interference (RFI) is a major concern for current and future systems, and extensive research in this topic has been reported in recent years (e.g., [1]–[10].) The current experience of significant RFI corruption of the observations of the SMOS radiometer [8], as well as the upcoming deployment of the Aquarius and SMAP missions [11], [12] motivate studies of the properties of the RFI environment as well as the performance of a variety of RFI detection and mitigation approaches.

A recent work [7] has reported results from an airborne L-band RFI observing system in Europe and Australia. The hardware utilized in [7] was capable of implementing algorithms for pulsed RFI detection using either a "pulse" or a full-band "kurtosis" detector, and statistics of RFI occurrences were described. However, the system used in [7] includes no frequency resolution, so that the detection of continuous interference of small to moderate intensity is limited. [9], [10] also report on airborne RFI observations in Europe that include both kurtosis and frequency resolution, but over a smaller set of observations than those of [7].

This paper presents new information on the RFI environment based on an airborne campaign conducted in conjunction with the Soil Moisture Active/Passive Validation Experiment 2008 (SMAPVEX08 [13]) to compile extensive RFI environment statistics, including observed RFI amplitude and source frequency characterization in the United States. The complete campaign included approximately 92 flight hours from September 20 to October 19, 2008. Only approximately 28 of these hours (see Table I) are considered in what follows due to the reduced utility of the remainder for RFI studies. The excluded portions consist of repeated overflights of soil moisture validation sites in Iowa or in Delaware, as well as an initial transit flight from Grand Junction, CO to Iowa when the full RFI observing system was not operated. Repeated observations of a geographic region are excluded given the goal of compiling statistics that are representative of a large geographical area. Fig. 1 illustrates the flight path for the remaining observations included in the study (excluding the 10/6/08 flight over the Delaware soil moisture site which is treated separately in what follows), and shows that the coverage of a moderately large geographic area is achieved by this data set. Total detected RFI levels in horizontal polarization are also illustrated in Fig. 1 when integrated to a 40-km spatial scale in a manner to be described in Section V.

Three RFI detecting and mitigating systems, the L-band interference suppressing radiometer (LISR) of Ohio State University (OSU) [1]–[3], [5], the agile digital detector (ADD, [4])

Manuscript received July 1, 2010; revised November 9, 2010; accepted December 20, 2010. This project was carried out under a contract with the National Aeronautics and Space Administration. The work performed by the University of Michigan was supported in part by NASA/JPL Award Reference Number 1335558.

J. Park, J. T. Johnson, N. Majurec, and N. Niamsuwan are with the Department of Electrical and Computer Engineering, The Ohio State University (OSU), Columbus, OH 43210 USA (e-mail: park.918@osu.edu; johnson@ece.osu.edu; majurec.1@osu.edu; niamsuwan.1@osu.edu).

J. R. Piepmeier and P. N. Mohammed are with the National Aeronautics and Space Administration (NASA), Goddard Space Flight Center, (GSFC), Greenbelt, MD 20771 USA (e-mail: jeffrey.r.piepmeier@nasa.gov; Priscilla.N.Mohammed@nasa.gov).

C. S. Ruf and S. Misra are with the Department of Atmospheric, Oceanic and Space Sciences, University of Michigan, Ann Arbor, MI 48109-2143 USA (e-mail: tgrs-editor@ieee.org; samisra@umich.edu).

S. H. Yueh and S. J. Dinardo are with the Jet Propulsion Laboratory, California Institute of Technology (Caltech), Pasadena, CA 91109 USA (e-mail: simon.h.yueh@jpl.nasa.gov; Steve.Dinardo@jpl.nasa.gov).

Color versions of one or more of the figures in this paper are available online at http://ieeexplore.ieee.org.

Digital Object Identifier 10.1109/TGRS.2011.2107560

TABLE I
SUMMARY OF THE FLIGHTS USED IN RFI ANALYSIS

Day	Location	Times (UTC)	Accum. Hours
9/26/08	Transit from Des Moines, IA to Cincinnati, OH	15:21~17:38	2.28
9/28/08	Transit from Cincinnati, OH to Newport News, VA	16:18~18:25	4.40
10/06/08	Delaware Site	12:12~16:18	8.50
10/07/08	RFI Survey (New Jersey, New York, Connecticut, Pennsylvania)	12:57~15:52	11.42
10/11/08	RFI Survey (DC area)	13:11~15:25	13.65
10/12/08	RFI Survey (DC area)	13:01~15:55	16.55
10/14/08	Transit from Wilmington to Atlanta, GA	12:50~16:47	20.50
10/16/08	RFI Survey (Circle around Atlanta, GA)	13:27~14:43	21.76
10/18/08	Transit from Atlanta, GA to Pittsburg, KS	13:02~16:25	25.14
10/18/08	Transit from Pittsburg, KS to Fort Collins, CO	19:59~22:57	28.10

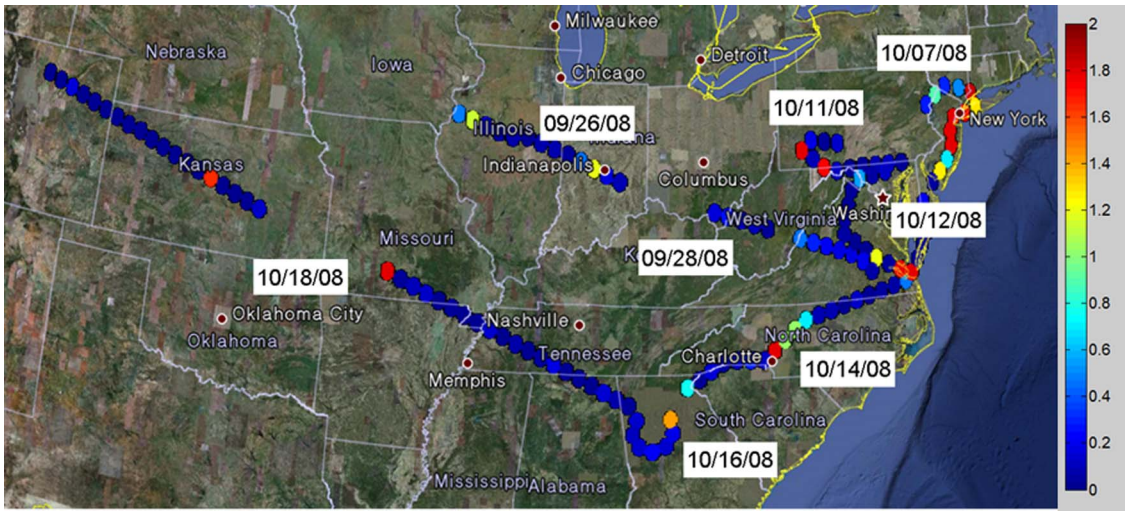

Fig. 1. Flight path utilized in RFI analysis (excluding 10/6/08 data). Geolocated RFI information at 40-km spatial resolution, horizontal polarization; colorscale in Kelvin.

of the University of Michigan (UM), and the "Analog Double Detector" (ADD) system [6] of NASA Goddard Space Flight Center (GSFC) were included in the campaign. These backend systems simultaneously observed intermediate frequency (IF) signals provided by the passive/active L-Band sensor (PALS) of Jet Propulsion Laboratory (JPL) [14], [15] installed on a Twin Otter aircraft.

The next section describes the instrument configuration in more detail, including the capabilities of each of the RFI systems, as well as the calibration methodology. Section III reviews the RFI detection and mitigation approaches applied, and observations for a set of specific RFI sources are then described in Section IV to provide further illustration of system capabilities and the RFI environment. The methods used to compile statistical information and the associated results are then discussed in Section V. A final analysis and overall conclusions are provided in Section VI. Note that portions of these results have been described previously [16]–[18], but this paper provides the first joint statistical analysis of the results from all the RFI observing systems in the campaign.

II. SYSTEM CONFIGURATION

A. PALS

PALS ([14], [15]) of JPL has been deployed in several remote sensing field campaigns in the past and has provided important information regarding the use of combined radar/radiometer instruments for observing several geophysical quantities while emphasizing soil moisture and sea surface salinity measurements in particular. Only the radiometer portion of PALS is considered here.

Fig. 2. Twin Otter aircraft (left) and RFI monitoring backend systems (right).

The PALS configuration for the campaign used a dual-polarized L-band patch array antenna having a two-sided 3-dB beamwidth of approximately 20°, similar to the configuration described in [14] and directed to produce a nominal 40° incidence angle on the earth surface. The antenna was mounted in a rear-facing orientation on the underside of a Twin Otter aircraft (Fig. 2) that was typically flown at altitudes ranging from 3 000 to 10 000 ft. Navigation data recorded by the PALS system is used in data processing to provide latitude, longitude, yaw, pitch, roll, and altitude information to enable footprint geolocation.

The relevant portion of the PALS radiometer front end has dual channels for the two polarizations; measured RF signals are filtered to occupy a 3-dB bandwidth of 1400–1420 MHz and are down converted by PALS to the 190–210 MHz 3-dB bandwidth IF signals provided to the RFI observing systems. The PALS frequency response has a ∼1397.5–1422.5 10-dB bandwidth, and a ∼1392–1426 MHz 20-dB bandwidth. These filter responses are somewhat wider than those used for satellite systems such as SMOS, making full-band PALS observations more susceptible to sources in bands slightly below the 1400–1427 MHz protected region. However, this filter response combined with the frequency resolution of the RFI observing systems is advantageous as it allows characterization of such sources.

PALS observations are switched through a sequence of internal load and noise diodes as well as the antenna inputs; a basic measurement is performed for 300 μsec out of a 350 μsec interval (the remaining 50 μsec is reserved for PALS radar measurements.) 12 of these 350 μsec measurements comprise one state observation lasting 4.2 ms (of which only 3.6 ms are used by the radiometer.) A sequence of 12 of these 4.2-ms intervals (50.4 ms) is repeated; the first seven intervals are antenna observations, while the remaining five involve internal reference load and noise diode measurements. The resulting final duty cycle of antenna observations is 50%. Control signals indicating the beginning of an integration period and the internal switch state are provided to the digital backend systems to synchronize operations.

B. OSU LISR

After an additional down conversion stage to translate the 200-MHz IF center frequency to 27 MHz, OSU LISR samples the IF at 100 MSPS using two 10-bit A/D converters (one for each polarization), and passes the resulting samples into an FPGA processor. The 50 MHz of bandwidth sampled for each polarization represents frequencies from 1385 to 1435 MHz. In the FPGA, samples from the two polarizations are combined into a single complex datastream occupying the bandwidths −50–0 MHz (vertical polarization) and 0–50 MHz (horizontal polarization.) A first pulse detection statistic is also computed by integrating the power of the time domain complex signal over 64 samples (0.64 μsec) and then "max-holding" this power over a 266.24 μsec integration period [5], [19]; the max-held quantity is recorded by the LISR computer for use in pulse detection postprocessing. The goal of this algorithm is the detection of pulsed interference of pulse durations comparable to the 0.64-μsec interval used.

A 1-K FFT is also performed on the data, and provides 1024 output frequencies (512 vertical and horizontal, respectively) every 10.24 μsec. The spectral resolution of the FFT is approximately 0.1 MHz, finer than most of the expected RFI sources. FFT outputs are then detected and integrated over 26 output spectra (a 266.24 μsec interval). Processing and output delays in the FPGA limit the observation to 266.24 μsec out of the available 300 μsec. The final LISR data unit thus consists of the power in 512 frequency channels for each polarization integrated over 266.24 μsec and reported in 32 bits, with an additional sample reporting the pulse detection statistic for this time period. The relatively high data rate of LISR also requires measurement dropouts associated with writing data to the internal storage system. The final net operating duty cycle of LISR is approximately 25% as compared to the 50% duty cycle of PALS antenna observations. A method for improving this duty cycle to the full 50% has been developed and will be utilized in future flights. However, the reduced duty cycle is not expected to produce a major impact on RFI statistical information due to the relatively low velocity of the Twin Otter aircraft, so that one footprint (and any associated RFI source) is typically observed for up to 30 s.

C. UM ADD

Similar to LISR, the UM ADD samples incoming horizontal and vertical polarization signals at a 17–37-MHz IF with eight-bit precision at 110 MSPS. Both polarization signals are then passed through eight-channel digital sub-band filters, and

cross-correlations between the polarizations are also computed [4]. The kurtosis [4] of each vertical and horizontal polarization sub-band signal is computed for purposes of RFI detection. In addition, full-band versions of the vertical and horizontal polarization signals are also cross-correlated and each of their kurtosis values is computed as well. Only the full-band kurtosis detection results are considered in this paper; these data are available for the full 50% duty cycle of the PALS antenna.

D. GSFC ADD

Unlike OSU LISR and UM ADD, the GSFC ADD observes IF signals provided from PALS without an additional down converter, and observes only in horizontal polarization. A tunnel diode detector with more than 20 MHz of video bandwidth is used to provide rapid sampling of the IF signal power; tunnel diode outputs are then passed to a video amplifier with a 125-kHz bandwidth. The GSFC-ADD system records 16-bit samples of this detected video at a 500-kHz sampling rate. In addition to this rapidly sampled power information, the GSFC ADD also includes a second detector system to produce a "pseudo-kurtosis" quantity [6] that is similar to the full-band kurtosis information recorded by the UM ADD. Due to these similarities, only the second moment data of the GSFC ADD system is utilized in what follows; these data are also available for the full 50% duty cycle of the PALS antenna.

E. Calibration

Data sets were recorded separately by each RFI observing system and by PALS, and were combined in postprocessing. Each data system included a GPS-based clock so that data sets could be aligned in time. Internal calibration standards using PALS reported internal calibration load brightnesses were applied to each data set individually, as well as a subsequent external calibration based on observations of water bodies. Since slight differences in assumptions about these quantities were used by the individual teams, a final cross-calibration was performed using PALS reported brightness temperatures from the 10/6/08 flight as the standard to which the remaining data sets were adjusted. The resulting corrections were found to be modest (gain corrections less than 2% for LISR and UM ADD, 7% for GSFC ADD), and produced only small impacts on observed RFI levels.

III. RFI Detection and Mitigation

The final joint data set consists of 266.24 μsec by 0.1-MHz spectrograms from OSU LISR, brightnesses and kurtosis values for horizontal and vertical polarizations from UM ADD (resolved in time at 4.1 ms), and horizontally polarized power sampled at 2 μsec from GSFC ADD. Horizontally and vertically polarized brightness temperatures from PALS resolved at 100 ms are also available for the 10/06/08 flight but were not available for the other flights utilized. In order to reduce the data volume, RFI and brightness temperature information was compiled first for a time interval of 1.5 s, corresponding to one LISR data file. Only time intervals for which all observing systems were operating were included (so that the final observing duty cycle is $\sim$25% as limited by LISR.)

The primary systems utilized for the detection of unambiguous "pulsed" RFI are the GSFC ADD (horizontal polarization) and OSU LISR (vertical polarization) measurements. Tests with the onboard LISR 0.64 μsec pulse detection algorithm showed relatively poor performance, indicating that the majority of pulsed interference observed apparently originates from pulsed sources with longer pulse lengths. Therefore, a second post-processing pulse detection algorithm was applied at 350 μsec time resolution (the resolution of the LISR spectrograms). Both the GSFC ADD and OSU LISR pulse detection approaches are similar, in that a set of power measurements (integrated over frequency for OSU LISR) within a time interval are sorted, and the mean and standard deviation of the lower 90% (lower 95% for GSFC) of the data are computed [2], [19]. The lower 90% or 95% are used in order to reduce the RFI contamination when calculating the mean and standard deviation. Samples exceeding a specified number of standard deviations from the mean power (seven standard deviations for OSU LISR and six standard deviations for GSFC) are declared pulses and excluded from subsequent integrations over time. The difference between total powers including or excluding these samples is then reported as the level of "pulsed" RFI detected. The false alarm rate for the OSU LISR detection algorithm is estimated at less than 0.25% due to the high threshold value used.

A "cross-frequency" algorithm [20] was also applied to the OSU LISR data after the application of the pulse detector. This algorithm uses the data versus frequency integrated to 1.5 s (one LISR datafile), using the PALS 10-dB bandwidth of $\sim$1398–1422 MHz. For each 1.5-s integration period, the mean of the lower $\sim$75% of these data is computed, and frequencies exceeding this mean by a threshold are classified as RFI corrupted and excluded from subsequent integrations over frequency and time. Subsequent integrations over frequency are weighted by a model of the PALS passband, so that the RFI levels computed are representative of those for the full-band observing instruments. The threshold level is nominally set to 100 K but is increased at the band edges in order to account for the reduced PALS gain (and increased NEDT) at these frequencies. The false alarm rate for this approach is less than 1%, and visual confirmation of the resulting RFI showed little evidence of significant false alarm impact.

The final RFI detection strategy uses the UM ADD full-band kurtosis [21]. In this case, deviations of the kurtosis from its expected value for Gaussian noise were computed at the 4.1-ms time interval of the original data. Samples more than four standard deviations from the expected value were classified as RFI; the associate false alarm rate is well below 1%. Detected RFI levels were again computed by comparing integrations including or excluding the detected samples. It is expected that the kurtosis approach should be very sensitive to short-pulsed RFI [21], [22], as well as other RFI types, although the sensitivity to more continuous RFI is reduced.

IV. RFI Examples

Selected examples of observed RFI sources are presented in this section to provide illustrative examples of the RFI environment as well as the joint system capabilities for detecting

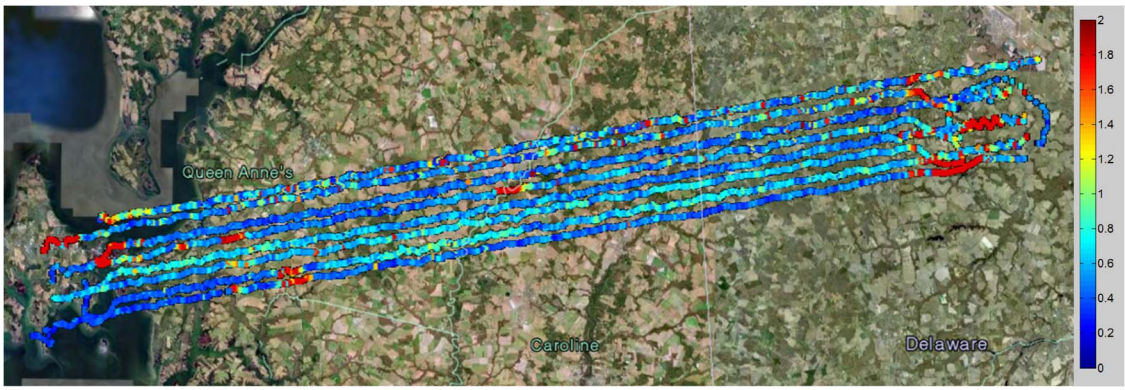

Fig. 3. Geolocated total LISR RFI detected, Oct. 6th, flight, horizontal polarization. colorscale in Kelvin.

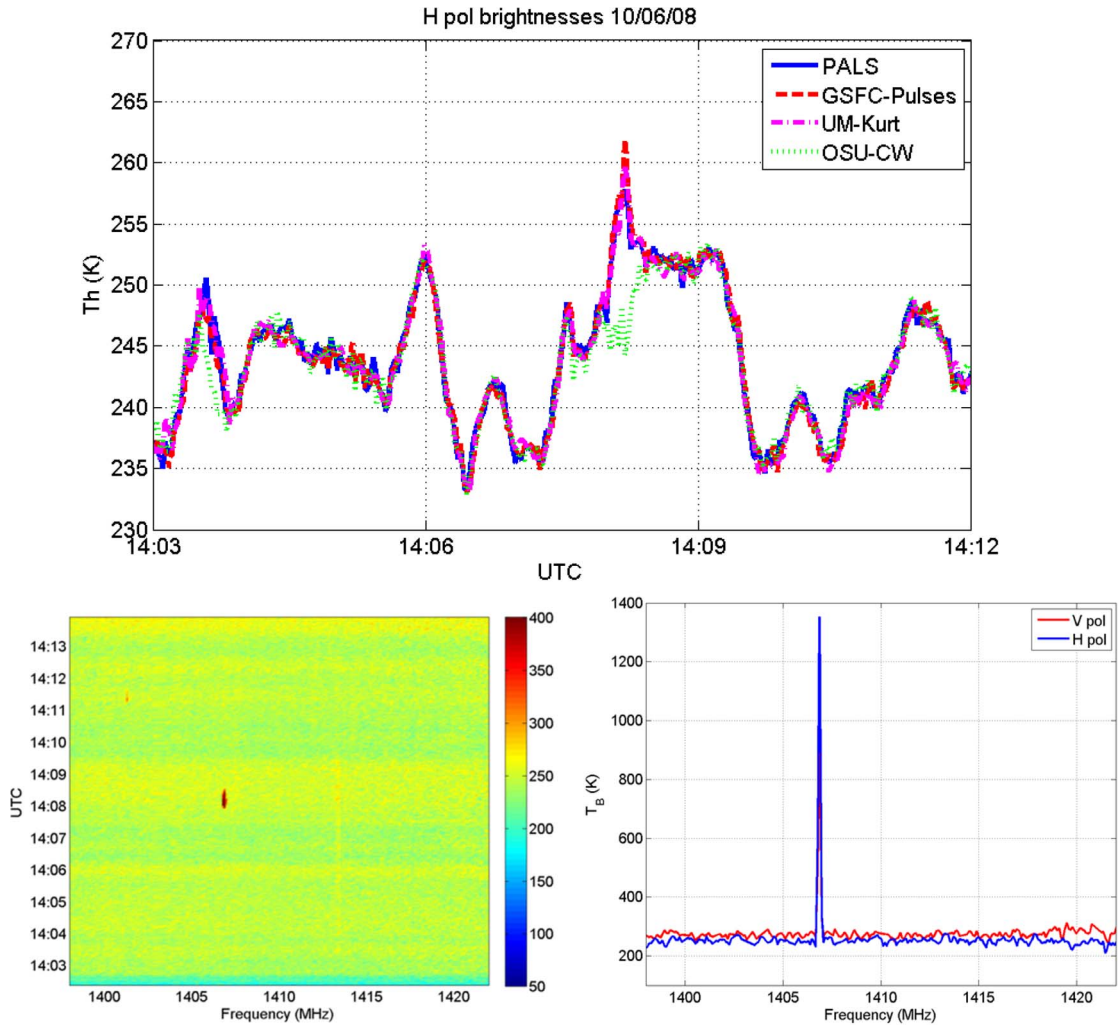

Fig. 4. Comparison of horizontally polarized brightness by PALS and three different digital backend systems (top), spectrogram of horizontally polarized brightness (bottom left), and horizontally polarized brightness versus frequency (bottom right).

RFI corruption. The first examples concentrate on the SMAPVEX08 soil moisture site observation of 10/6/08 because PALS data sets were available for intercomparison on this date. Fig. 3 provides a map of the flight path on 10/6/08, which consists of repeated passes over a portion of soil moisture ground truthing sites in Delaware and Maryland. The associated horizontally polarized RFI level detected by OSU LISR (sum of cross-frequency and pulse algorithms) is also illustrated, and shows that significant RFI is present on the edges of each flight line as well as in other isolated locations. Fig. 4 (top) presents comparisons of the horizontally polarized brightnesses from 14:03–14:12 UTC, during which the aircraft is moving eastward along the fourth line from the north. Fig. 4 demonstrates the success of the data alignment and calibration, given the good agreement among the observations of the multiple systems.

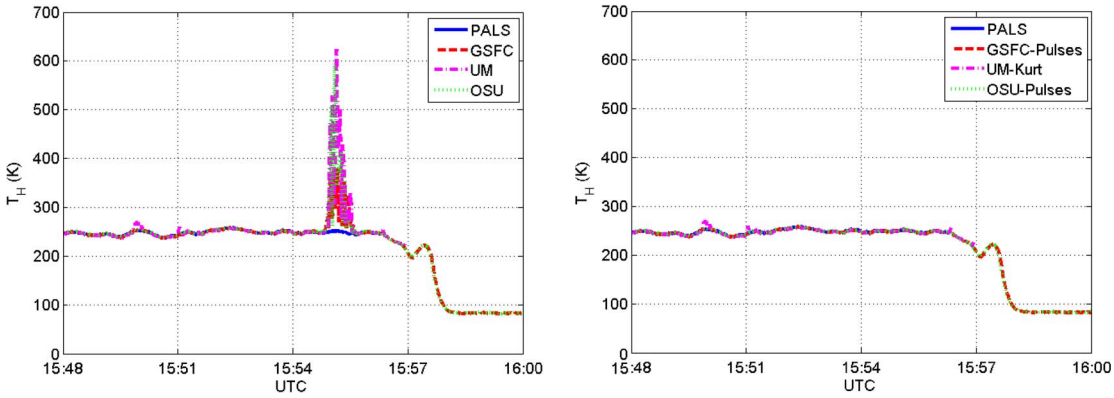

Fig. 5. Comparison of detected pulsed RFI by PALS, GSFC ADD, UM ADD and OSU LISR. The left panel shows the unprocessed measurements and the right panel shows the results after RFI mitigation algorithms have been applied.

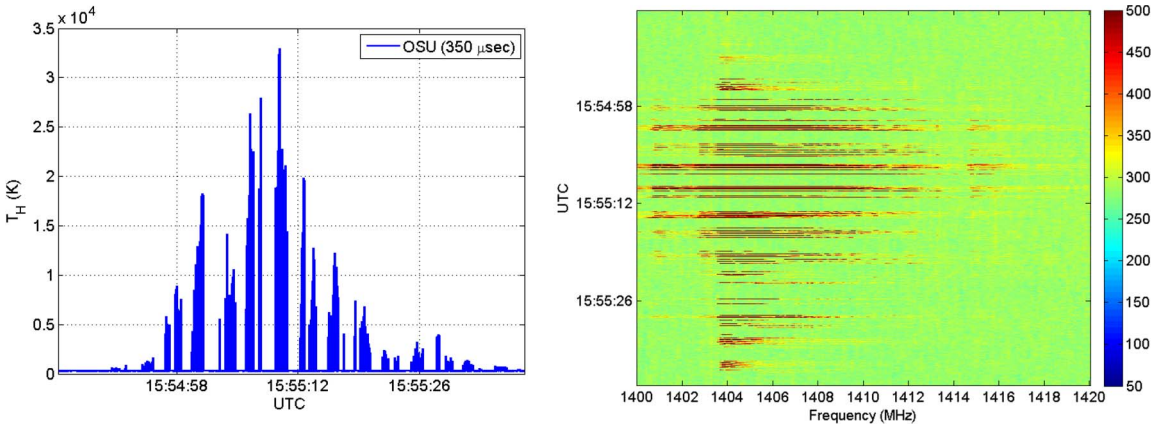

Fig. 6. Horizontally polarized brightness at 350-μsec time resolution versus UTC (left), spectrogram of horizontally polarized brightnesses at 22.4-msec time resolution (right).

The data sets shown are those following application of the associated RFI detection and mitigation strategies, which primarily show the absence of RFI during this interval of time. However, larger differences at time ∼14:08 are observed, with the OSU LISR mitigated data showing brightness up to ∼10 K lower than those of the other systems. An examination of the LISR spectrogram in the lower portion of Fig. 4 shows the presence of narrowband RFI near a frequency of 1407 MHz (14:08 UTC). The bottom-right plot of brightness temperature versus frequency at 14:08 UTC shows narrowband RFI exceeding 1000 K near 1407 MHz as the source of the ∼10 K change in the full-band brightness temperature. The source producing this emission remains to be identified, but would be difficult to distinguish from natural geophysical variations without the use of frequency resolution due to its narrowband and continuous nature.

Example observations of a pulsed RFI source near the eastern edge of the flight path are provided in Fig. 5; strong RFI near time 15:55 UTC is observed in the unprocessed data for all instruments, which is then successfully mitigated by all the detection algorithms applied (right). Note that the PALS system also employs a pulsed RFI detection strategy similar to that described in Section III and applied at 0.1-s time resolution. The good agreement of the mitigated data from the multiple observing systems even during transition from land to water surface observation at later times (i.e., greater than

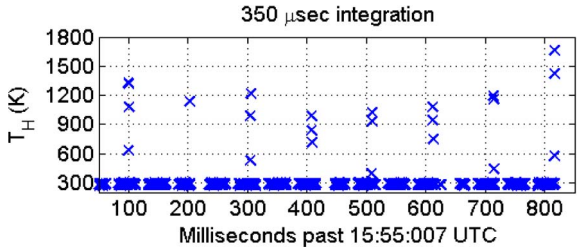

Fig. 7. Pulsed RFI detected by 350-μsec pulse blanker corresponding to Figs. 5 and 6 over a time interval less than 1 s.

15:57 UTC) provides further evidence of the fidelity of the intercomparison.

Additional analysis of this source using OSU LISR data is provided in Figs. 6 and 7. The left-hand portion of the former "zooms" the 350 μsec LISR data set in time near the RFI source, and the associated spectrogram is shown in the right plot. The pulsed interference observed is of a broad band nature, and exceeds 30 000 K full-band brightness temperature in some cases when resolved at 350-μsec time resolution. An additional higher time resolution plot in Fig. 7 shows an apparent pulse repetition interval of approximately 102 ms. Again, the source of these emissions remains unidentified.

The remaining examples considered arise from the transit and dedicated RFI observing flights; the 10/6/08 observations are excluded from the statistical analyses to be reported in

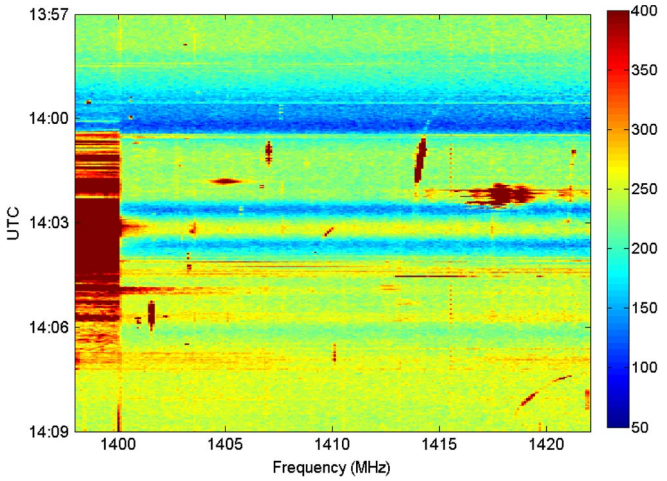

Fig. 8. Spectrogram of horizontally polarized brightness during New York City overflight (prior to application of cross-frequency mitigation algorithm and pulse detection algorithm) Oct. 7th.

Section V due to the repeated observations of a small geographical area that they represent.

The October 7th flight included a direct overpass of New York City (see Fig. 1). Fig. 8 is the OSU LISR spectrogram in horizontal polarization for the portion of the flight including an overpass of Manhattan. This spectrogram shows a very strong source from 1398 to 1400 MHz; additional analysis of the spectrogram at frequencies down to 1390 MHz shows a set of ∼2-MHz wide interferers suggestive of a channelized communications systems. This application is consistent with frequency allocation regulations in the United States. Numerous other in-band sources are also observed including apparent frequency modulated sources near 1414 (14:00–14:03 UTC) and 1420 MHz (14:06–14:09 UTC). Fig. 9 illustrates full-band brightness temperatures before and after application of RFI mitigation algorithms for this period with the UM ADD, GSFC ADD, and OSU LISR data sets, respectively. Full-band brightnesses exceeding 1000 K are observed in the top and the middle panels of Fig. 9, primarily due to the strong impact of the 1390–1400 MHz sources, with only a moderate impact of the pulse and kurtosis detection algorithms due to the more continuous nature of these sources, for which the interference to noise ratio (before calibration) is approximately −3 dB. OSU LISR data in the bottom panel of Fig. 9 was computed using only the frequency range 1400–1422 MHz (for this time period only), so that the strong communications source was excluded, and a maximum "full-band" brightness for this spectral range of ∼450 K is obtained. Subsequent application of pulse and cross-frequency detection algorithms to this strategy produces the RFI mitigated results of Fig. 9 (bottom) that appear more realistic. Fig. 10 summarizes the pulsed (left) and cross-frequency (right) detected RFI levels for this portion of the flight; low-level pulsed RFI is observed throughout, while the impact of cross-frequency detected RFI exceeds 1 K in only a few time intervals. These results demonstrate the ability of the combined system to detect and remove RFI even in challenging environments.

An additional example of a very strong RFI source is provided in Fig. 11, recorded during a portion of the October

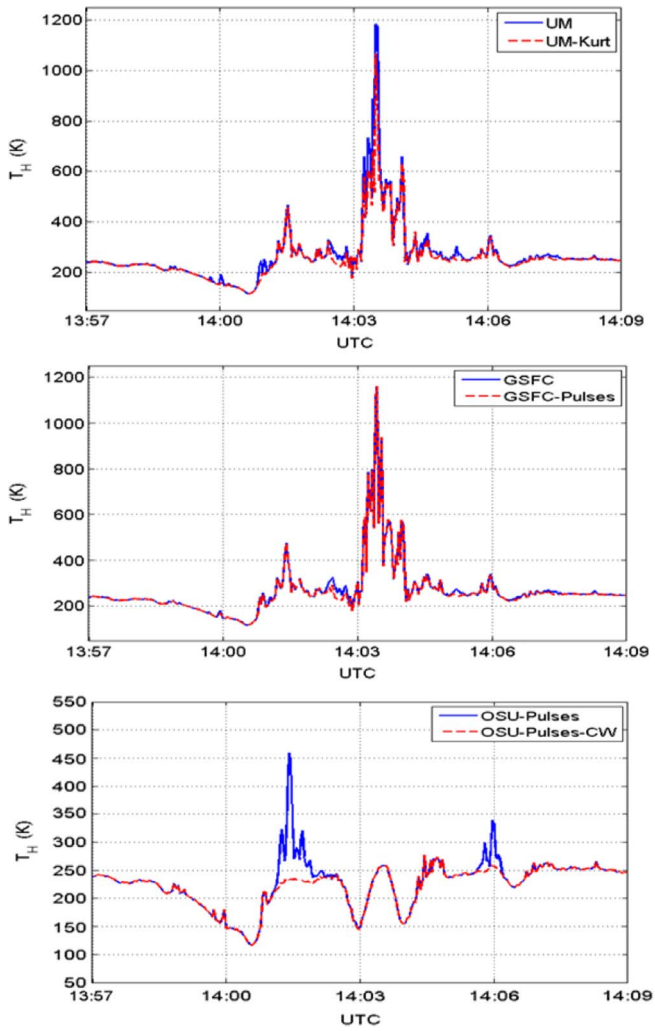

Fig. 9. Comparison of horizontally polarized brightness for the time interval of Fig. 8 prior to and following UM Kurtosis detection and mitigation algorithm (top), GSFC pulse detection and mitigation algorithm (middle), and cross-frequency mitigation algorithm (bottom.).

18th flight that passed within 1.5 km of a Digital Television (DTV) Channel 52 transmitter in Springfield, MO. Channel 52 transmitters in the United States at this time used frequencies 698–704 MHz, so that the second harmonic of the transmission occupies 1396–1408 MHz. Clear evidence of this second harmonic is observed; this information can be used to assess the level of second harmonic emissions from the transmitter. Note that following the DTV transition in the United States, 698–704 MHz is no longer allocated to television transmissions, but rather to personal communications systems. However, the example remains illustrative of the potential effects of second harmonic emissions into L-band. Fig. 12 illustrates the individual full-band horizontally polarized observations of the UM ADD, GSFC ADD, and OSU LISR systems, and again shows the difficulties of detecting and mitigating this strong source using pulsed or kurtosis approaches when the full-band data alone are used. In this case, the use of the ADD frequency sub-band channels would be more appropriate, as their use permits the RFI to be isolated in particular sub-bands and then mitigated by selective removal of the contaminated sub-bands. The cross-frequency strategy, which discards much of

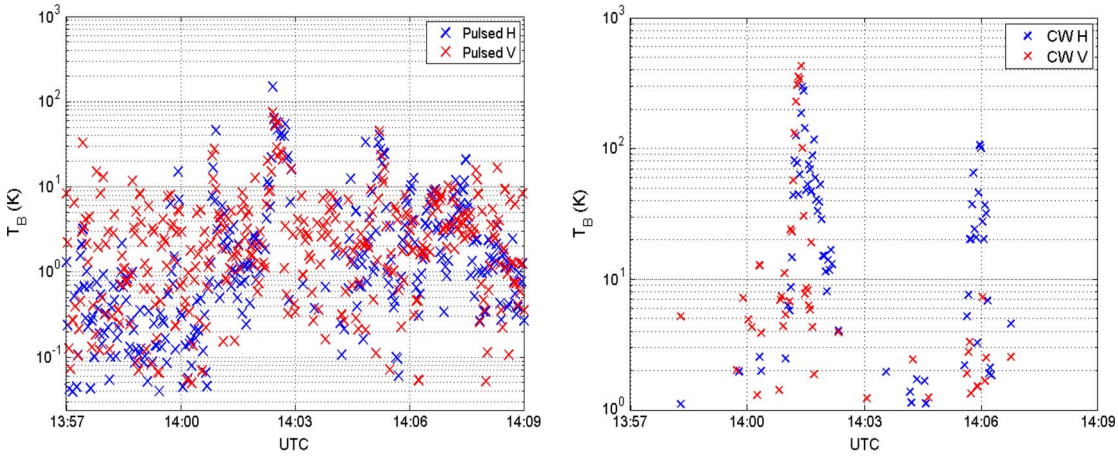

Fig. 10. OSU LISR detected pulsed (left) and CW (right) RFI corresponding to Figs. 8 and 9.

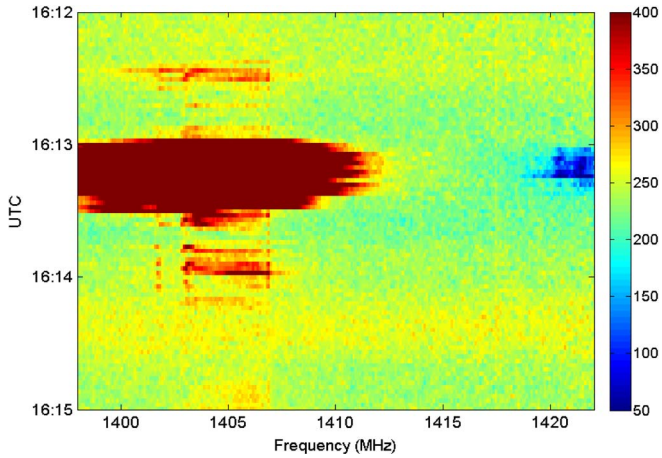

Fig. 11. Spectrogram of horizontally polarized brightnesses during Springfield, MO overflight (prior to application of cross-frequency mitigation algorithm and pulse detection algorithm) Oct. 18th.

the radiometer bandwidth in some portions of the observation is more successful in removing this source, although some apparent interference remains.

An additional analysis of this source is reported in Fig. 13, using the known antenna location and transmit power, as well as a description of the PALS antenna pattern and orientation. Received brightness temperatures predicted by the Friis transmission formula versus range are found to provide a reasonable match to the measured data. An assumption of a second harmonic suppression of 98 dB, which falls within legal limits, was used to produce these results.

V. RFI Statistics

While the RFI examples presented in Section IV provide some evidence of both strong and weak RFI sources and their properties, the extensive data set obtained prohibits an exhaustive examination of all RFI events. Statistics of RFI levels detected by pulsed algorithms (GSFC and OSU LISR for horizontal and vertical polarization, respectively) cross-frequency (OSU LISR) and full-band kurtosis (UM ADD) approaches were compiled using 32416 datapoints representing 1.5-s time integrations. Fig. 14 plots the resulting RFI distribution functions in terms of the percent chance (vertical axis) of exceeding the RFI level specified on the horizontal axis.

The pulsed algorithm curves show significant RFI corruption that is stronger in vertical polarization at low RFI levels but more similar between polarizations at larger RFI levels. The sum of pulsed and cross-frequency detected RFI is represented by the OSU "total" curves, showing that significant cross-frequency RFI is also present, and that RFI levels exceeding 1 K at these scales is experienced $\sim$7 to 8% of the time, while RFI exceeding 10 K is experienced $\sim$1% of the time. Full-band kurtosis detected RFI is slightly larger than that of the OSU system at RFI levels < 0.5 K, possibly indicating the presence of short pulses for which the full-band kurtosis approach is more sensitive. Alternatively, the full-band kurtosis detected RFI is less than the LISR total at high RFI levels, likely due to the algorithm's reduced sensitivity for more continuous RFI types.

Averaging these observations to larger spatial scales is desirable in order to predict RFI levels for satellite missions. This is because an analysis of the Friis transmission formula for satellite observations shows that it is the "density of interferers" that is relevant for predicting RFI corruption, even given the differing antenna patterns, etc. between ground and space-based observations. Instantaneous PALS antenna observations typically represent a footprint of $\sim 1.84 \times 0.87$ km at the nominal flight altitude of 3 km. Averaging these observations over along track distances of 40 km provides spatial scales in one dimension representative of a satellite antenna footprint diameter. However, the cross-track dimension of this averaged spot remains < 1 km; an additional assumption that the regions of interest are statistically homogeneous over a 40-km cross-track scale is then required for predicting expected satellite RFI levels. This assumption is believed preferable to an integration over a satellite footprint area, given the limited amount of data available and the variety of geographical regions that would be combined in such a process.

Fig. 15 presents the RFI distribution functions following the 40-km linear integration (101 remaining points). Results are qualitatively similar to those in Fig. 14, except that the percentage of points having lower level RFI is somehow increased. CW RFI levels occur more frequently than pulsed RFI

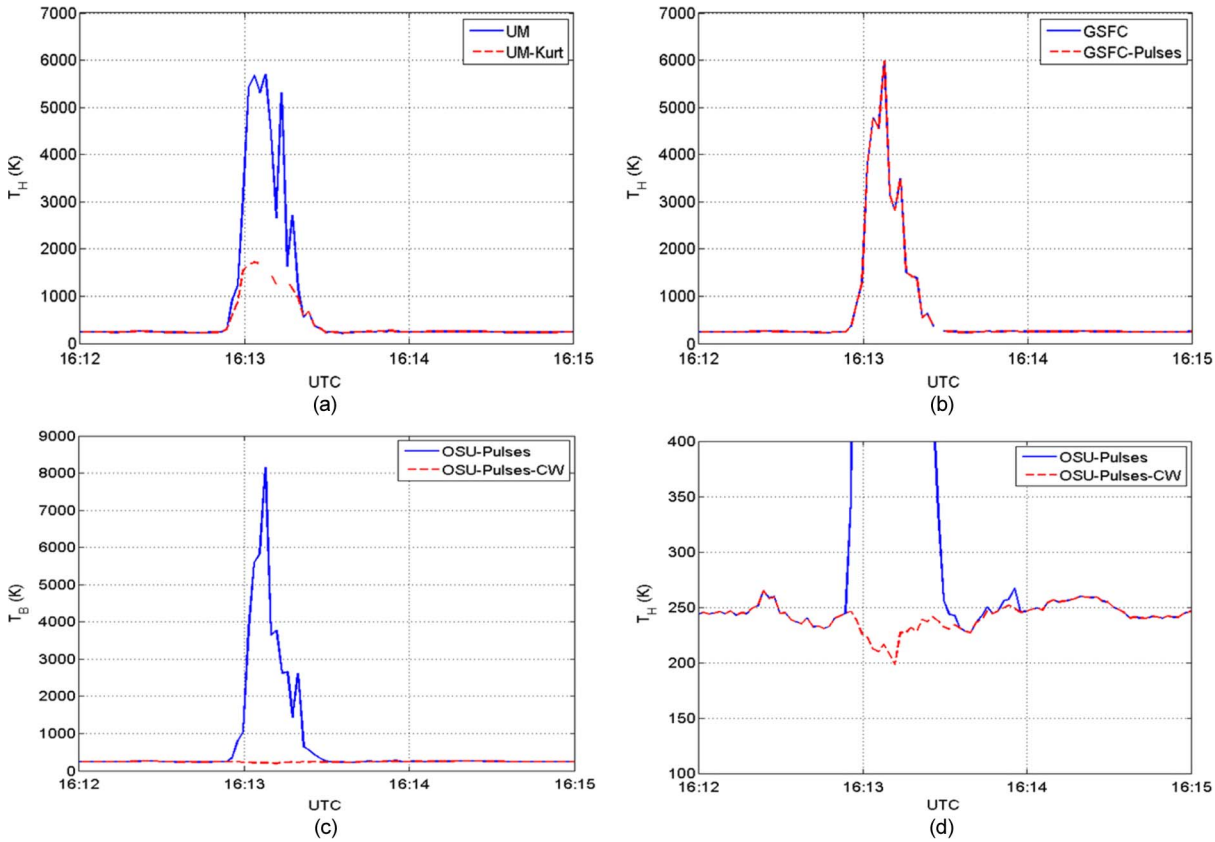

Fig. 12. Comparison of horizontally polarized brightness prior to and following UM Kurtosis (top left), GSFC pulse detection (top right), and OSU cross-frequency mitigation algorithm (bottom).

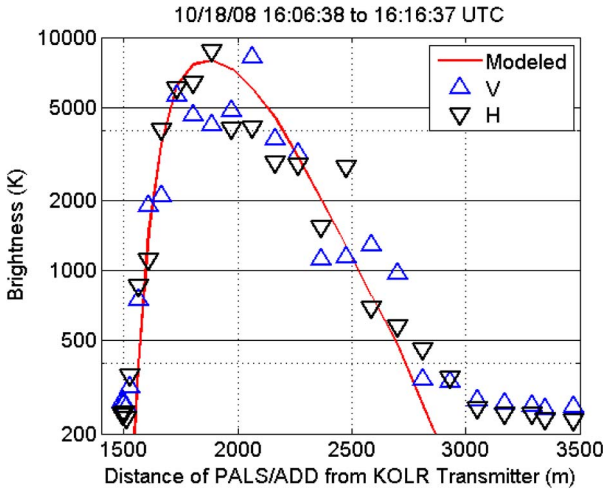

Fig. 13. Brightness versus distance of PALS/ADD from KOLR transmitter compared with predictions of the Friis transmission formula (labeled "modeled").

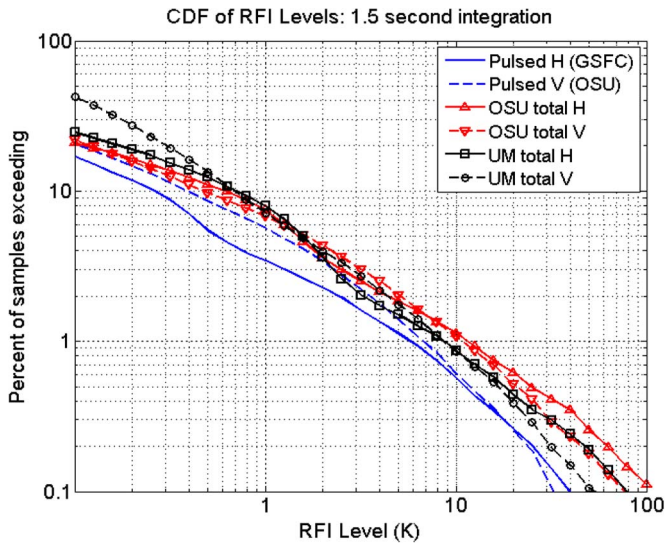

Fig. 14. RFI distribution functions detected in vertical and horizontal polarizations by OSU LISR, UM ADD, and GSFC ADD (32416 1.5-s time intervals.).

at large power levels, although the largest cases are dominated by the specific sources considered in Figs. 8 and 11. In general, these results show that RFI at low to moderate power levels is not uncommon in the United States, and must be addressed if radiometric data is to have sufficient quality for precision scientific applications.

Due to these issues, the NASA SMAP mission is currently implementing a digital backend to enhance the detection and mitigation of RFI. This system will include time-, frequency-, and kurtosis-based strategies as considered in this experiment. However, the 512 spectral channels per polarization achieved by OSU LISR are not practical for a satellite downlink, so that a reduced number of spectral channels (currently baselined at 16) will be used. In order to assess the potential performance of such a system for detecting frequency localized RFI, an additional study was performed using the 101 40-km integrated LISR spectrograms. The spectrograms were integrated in

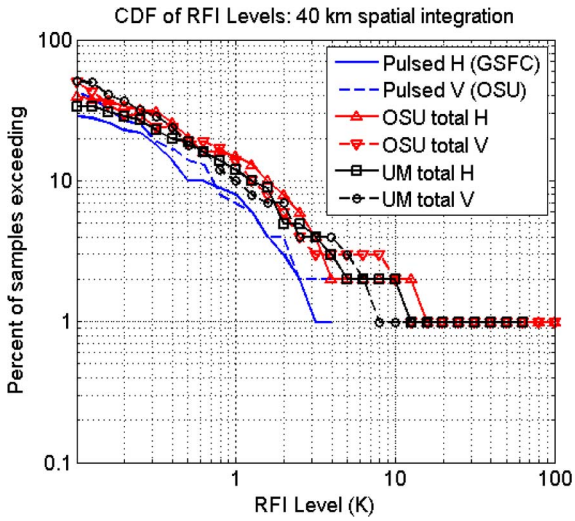

Fig. 15. Histogram for the campaign of RFI levels detected in vertical and horizontal polarizations by OSU LISR, UM ADD, and GSFC ADD. Results for 40-km spatial integration (101 40 km spatial intervals).

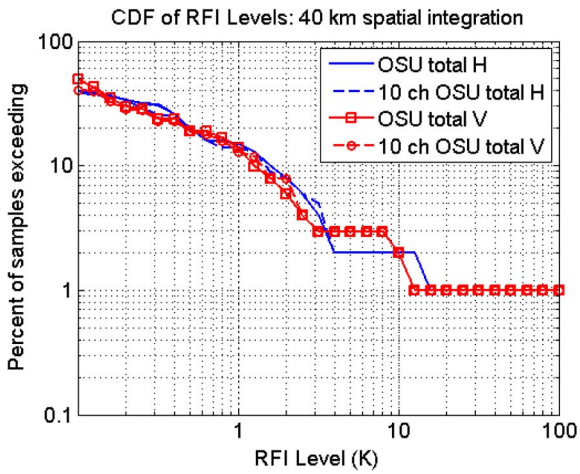

Fig. 16. Histogram for the campaign of total RFI levels detected in vertical and horizontal polarizations by OSU LISR. Results for OSU in-band channels and averaged 10 channels (101 40-km spatial intervals).

frequency to produce ten 1.5-MHz channels (the center 15 MHz of the PALS passband to reduce passband effects), and the cross frequency algorithm applied to this reduced resolution data set. In this process, additional Gaussian noise of 4 K was added to each of the 10 subchannels in order to model the expected SMAP radiometer sensitivity of 1 K in the full-band observation. The resulting RFI distribution function is compared with that using the full spectral resolution in Fig. 16. The general similarity of the detected RFI levels shows that the reduced spectral resolution approach should be successful in detecting and mitigating RFI of the type observed in the campaign of this paper.

VI. Conclusion

RFI observations from an airborne campaign covering geographically diverse portions of the United States were presented in this paper. The multiple digital backends included in the campaign each provided distinct RFI detection and mitigation approaches, and each was shown to provide advantages for particular source types. The value of multiple frequency channels, as opposed to the previous European/Australian campaign results reported in [7], was also demonstrated. Selected RFI examples including both strong and weak sources were examined, and included definitive observation of second harmonic emissions from a licensed source operating under legal limits. The statistical information presented in Section V showed that RFI corruption of L-band radiometer observations at low to moderate power levels is likely in the United States; for example, RFI exceeding 1 K is forecasted to occur in 10%–20% of observations. The difficulties in detecting such low-level RFI with traditional radiometer approaches motivate the use of dedicated RFI strategies in future satellite missions such as SMAP. Note that these results are consistent with currently available RFI information from the SMOS mission, for which only the largest RFI sources (i.e., $>$ ∼50–100 K) are easily detectable at present, and which are largely absent from the continental United States. Future work with SMOS observations will be required to address approaches for detecting and removing this low-level RFI and its effect on SMOS science applications.

References

[1] G. A. Hampson, S. W. Ellingson, and J. T. Johnson, "Design and demonstration of an interference suppressing microwave radiometer," in *Proc. IEEE Aerosp. Conf.*, 2004, vol. 2, pp. 993–999.

[2] N. Niamsuwan, J. T. Johnson, and S. W. Ellingson, "Examination of a simple pulse blanking technique for RFI mitigation," *Radio Sci.*, vol. 40, p. RS5S03, Jun. 2005.

[3] J. T. Johnson, A. J. Gasiewski, B. Guner, G. A. Hampson, S. W. Ellingson, R. Krishnamachari, N. Niamsuwan, E. McIntyre, M. Klein, and V. Leuski, "Airborne radio frequency interference studies at C-band using a digital receiver," *IEEE Trans. Geosci. Remote Sens.*, vol. 44, no. 7, pp. 1974–1985, Jul. 2006.

[4] C. S. Ruf, S. M. Gross, and S. Misra, "RFI detection and mitigation for microwave radiometry with an agile digital detector," *IEEE Trans. Geosci. Remote Sens.*, vol. 44, no. 3, pp. 694–706, Mar. 2006.

[5] B. Guner, N. Niamsuwan, and J. T. Johnson, "Time and frequency blanking for RFI mitigation in microwave radiometry," *IEEE Trans. Geosci. Remote Sens.*, vol. 45, no. 11, pp. 3672–3679, Nov. 2007.

[6] J. R. Piepmeier, P. Mohammed, and J. Knuble, "A double detector for RFI mitigation in microwave radiometers," *IEEE Trans. Geosci. Remote Sens.*, vol. 46, no. 2, pp. 458–465, Feb. 2008.

[7] N. Skou, S. Misra, J. E. Balling, S. S. Kristensen, and S. S. Sobjaerg, "L-band RFI as experienced during airborne campaigns in preparation for SMOS," *IEEE Trans. Geosci. Remote Sens.*, vol. 48, no. 3, pp. 1398–1407, Mar. 2010.

[8] J. E. Balling, S. S. Sobjaerg, S. S. Kristensen, and N. Skou, "RFI and SMOS: Preparatory campaigns and first observations from space," in *Proc. MICRORAD*, 2010, pp. 282–287.

[9] M. Pardé, M. Zribi, P. Fanise, M. Dechambre, J. Boutin, N. Reul, J. Tenerelli, D. huser, and Y. Kerr, "Radio frequency interference investigation using the airborne L-band full polarimetric radiometer CAROLS," in *Proc. MICRORAD*, 2010, pp. 300–305.

[10] P. Fanise, M. Zribi, M. Pardé, and M. Dechambre, "Elimination of RFI noise in CAROLS radiometer data using a hardware detector," presented at the Microwave Radiometry and Remote Sensing of the Environment (MicroRad), Washington, DC, 2010.

[11] G. Lagerloef, F. R. Colomb, D. Le Vine, F. Wentz, S. Yueh, C. Ruf, J. Lilly, J. Gunn, Y. Chao, A. de Charon, and C. Swift, "The Aquarius/SAC-D mission: Designed to meet the salinity remote-sensing challenge," *Oceanography*, vol. 21, no. 1, pp. 68–81, Mar. 2008.

[12] D. Entekhabi, E. G. Njoku, P. E. O'Neill, K. H. Kellogg, W. T. Crow, W. N. Edelstein, J. K. Entin, S. D. Goodman, T. J. Jackson, J. Johnson, J. Kimball, J. R. Piepmeier, R. D. Koster, N. Martin, K. C. McDonald, M. Moghaddam, S. Moran, R. Reichle, J. C. Shi, M. W. Spencer, S. W. Thurman, and J. Van Zyl, "The soil moisture active passive (SMAP) mission," *Proc. IEEE*, vol. 98, no. 5, pp. 704–716, May 2010.

[13] Soil Moisture Active Passive Validation Experiment, 2008. [Online]. Available: http://www.ars.usda.gov/Research/docs.htm?docid=17526&page=1

[14] S. Yueh, W. Wilson, E. Njoku, S. Dinardo, D. Hunter, Y. Rahmat-Samii, K. S. Kona, and M. Manteghi, "Compact, lightweight dual-frequency microstrip antenna feed for future soil moisture and sea surface salinity missions," in *National Aeronautics and Space Administration (NASA) Earth-Sun System Technology Conf.*, College Park, MD, 2006.

[15] S. Yueh, S. Dinardo, A. Fore, and F. Li, "Passive and active L-band microwave observations and modeling of ocean surface winds," *IEEE Trans. Geosci. Remote Sens.*, vol. 48, no. 8, pp. 3087–3100, Aug. 2010.

[16] N. Majurec, J. Park, N. Niamsuwan, M. Frankford, and J. T. Johnson, "Airborne L-band RFI observations in the SMAPVEX08 campaign with the L-band Interference Suppressing Radiometer," in *Proc. IEEE Geosci. Remote Sens. Symp.*, 2009, pp. II-158–II-161.

[17] S. Misra and C. S. Ruf, "Characterization of L-band RFI across the continental USA using a kurtosis detector," presented at the IEEE Geoscience Remote Sensing Symp., Cape Town, South Africa, 2009.

[18] J. T. Johnson, J. R. Piepmeier, C. Ruf, and S. Yueh, "L-band RFI airborne observations," presented at the Microwave Radiometry and Remote Sensing of the Environment (MicroRad), Washington, DC, 2010.

[19] J. T. Johnson and L. C. Potter, "A study of detection algorithms for pulsed sinusoidal interference in microwave radiometry," *IEEE Trans. Geosci. Remote Sens.*, vol. 47, no. 2, pp. 628–636, Feb. 2009.

[20] B. Guner and J. T. Johnson, "Performance study of a cross-frequency detection algorithm for pulsed sinusoidal RFI in microwave radiometry," *IEEE Trans. Geosci. Remote Sens.*, vol. 48, no. 7, pp. 2899–2908, Jul. 2010.

[21] R. D. De Roo, S. Misra, and C. S. Ruf, "Sensitivity of the kurtosis statistic as a detector of pulsed sinusoidal RFI," *IEEE Trans. Geosci. Remote Sens.*, vol. 45, no. 7, pp. 1938–1946, Jul. 2007.

[22] S. Misra, P. N. Mohammed, B. Guner, C. S. Ruf, J. R. Piepmeier, and J. T. Johnson, "Radio frequency interference detection algorithms in microwave radiometry: A comparative study," *IEEE Trans. Geosci. Remote Sens.*, vol. 47, no. 11, pp. 3742–3754, Nov. 2009.

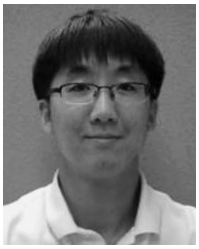

James Park (S'09) received the B.S. degree in electronics engineering from Konkuk University, Seoul, Korea, in 2007. He is currently working toward the Ph.D. degree at the Ohio State University (OSU), Columbus.

He is currently a Graduate Research Associate in the ElectroScience Laboratory, the Ohio State University, Columbus. His research interests include microwave remote sensing and electromagnetic wave theory.

J. T. Johnson (S'88–M'96–SM'03–F'09) received the bachelor of electrical engineering degree from the Georgia Institute of Technology, Atlanta, in 1991 and the S.M. and Ph.D. degrees from the Massachusetts Institute of Technology (MIT), Cambridge, in 1993 and 1996, respectively.

He is currently a Professor in the Department of Electrical and Computer Engineering and ElectroScience Laboratory of The Ohio State University (OSU), Columbus. His research interests are in the areas of microwave remote sensing, propagation, and electromagnetic wave theory.

Dr. Johnson is a member of commissions B and F of the International Union of Radio Science (URSI), and a member of Tau Beta Pi, Eta Kappa Nu, and Phi Kappa Phi. He received the 1993 best paper award from the IEEE Geoscience and Remote Sensing Society, was named an Office of Naval Research Young Investigator, National Science Foundation Career awardee, and PECASE award recipient in 1997, and was recognized by the U. S. National Committee of URSI as a Booker Fellow in 2002.

Ninoslav Majurec received the B.S. and M.S. degrees in electrical engineering from Faculty of Electrical Engineering and Computing, University of Zagreb, Zagreb, Croatia, in 1996 and 1999, respectively, and the Ph.D. degree in electrical engineering from University of Massachusetts, Amherst, in 2008.

He is currently a Senior Research Associate with the ElectroScience Laboratory, The Ohio State University (OSU), Columbus. His research interests include remote sensing, software-defined radars, MIMO radars, microwave radiometers, multi-frequency (microwave and millimeter wave) radar systems, SAR systems and SAR image processing, digital receivers, and data acquisition systems and microwave measurements. His current research interests include electromagnetic simulations of ocean scattering.

Noppasin Niamsuwan (S'04–M'05) received the B.Eng. degree in electrical and electronic engineering from the Asian University of Science and Technology, Chonburi, Thailand, in 2003, and the M.S. and Ph.D. degrees in electrical engineering from The Ohio State University (OSU), Columbus, in 2005 and 2009, respectively.

He is currently a Postdoctoral Scholar with Jet Propulsion Laboratory, California Institute of Technology, Pasadena. His research interests include microwave remote sensing, electromagnetic wave theory, remote sensing of earth's surface and atmosphere.

Dr. Niamsuwan is a member of IEEE and American Geophysical Union.

Jeffrey R. Piepmeier (S'95–M'99) received the Ph.D. degree in electrical engineering from Georgia Institute of Technology, Atlanta, in 1999. Previously, he received the M.S. degree in electrical engineering from Georgia Tech in 1994 and the B.S. degree in engineering from LeTourneau University, Longview, TX, in 1993.

From 1993 to 1994, he was a Schakleford Fellow with the Georgia Tech Research Institute. Piepmeier was third place winner in the 1998 IGARSS student prize paper competition. In 1999, he was with the Microwave Instrument Technology Branch at NASA's Goddard Space Flight Center, Greenbelt, MD. There he has been principle and co-investigator on several technology-development projects in microwave radiometry and RFI mitigation. Currently he is instrument system engineer for the NASA's Aquarius radiometer and instrument scientist for the SMAP radiometer and GPM Microwave Imager.

Dr. Piepmeier was recipient of an Excellence in Federal Career Gold Award (Rookie-of-the-year) in 2000 and was conference chair of the 2000 Microwave Radiometer Calibration Workshop (MicroCal2000). He was a 2002 NASA Earth Science New Investigator. He received the NASA/GSFC Exceptional Achievement Award and Technology Advancement Award in 2005 and 2007, respectively. Dr. Piepmeier is a member of IEEE, URSI (Commission F), and the American Geophysical Union. He is a past Chair of the GRSS Instrumentation and Future Technologies technical subcommittee. Currently, he serves as Chairperson of the National Academies' Committee on Radio Frequencies (CORF).

Priscilla N. Mohammed (S'02–M'06) received the Ph.D. degree in electrical engineering and a Master's degree in electrical engineering both from the Georgia Institute of Technology, Atlanta, in 2005 and 2001, respectively and a B.S. degree in electrical engineering from the Florida Institute of Technology, Melbourne, in 1999.

As a Ph.D. student, Priscilla performed microwave measurements of gaseous phosphine and ammonia u nder simulated conditions for the outer planets and used these measurements to develop a radio occultation simulator to predict absorption and excess Doppler due to Saturn's atmosphere. Much of this work was in support of the Cassini mission to Saturn. Based on these laboratory results, the Cassini Project Science Group made the decision to extend the Ka-band (32 GHz) operation throughout the mission tour. The predicted attenuation profiles for the Cassini radio occultation maneuver of May 2005, earned her an invitation by the Cassini Radio Science Team to present a paper on their behalf at the 37th Annual Meeting of the Division for Planetary Sciences in Cambridge, England. In 2006 she was with the Goddard Earth Sciences and Technology Center at the University of Maryland, Baltimore County, as a member of their research faculty. Since joining GEST she has done research and published in the field of radio frequency interference mitigation in microwave radiometers. She is currently the Level 1B science algorithm team lead for the Soil Moisture Active and Passive (SMAP) mission which encompasses space flight application of her research.

Christopher S. Ruf (S'85–M'87–SM'92–F'01) received the B.A. degree in physics from Reed College, Portland, OR, and the Ph.D. degree in electrical and computer engineering from the University of Massachusetts, Amherst.

He is currently a Professor of atmospheric, oceanic, and space sciences; a Professor of electrical engineering and computer science; and Director of the Space Physics Research Laboratory, University of Michigan, Ann Arbor. He has worked previously at Intel Corporation, Hughes Space and Communication, the NASA Jet Propulsion Laboratory, Pasadena, CA and Penn State University. In 2000, he was a Guest Professor with the Technical University of Denmark (DTU), Lyngby. He has published in the areas of microwave radiometer satellite calibration, sensor and technology development, and atmospheric, oceanic, land surface, and cryosphere geophysical retrieval algorithms.

Dr. Ruf is a member of the American Geophysical Union (AGU), the American Meteorological Society (AMS), and Commission F of the Union Radio Scientifique Internationale. He has served on the editorial boards of the AGU *Radio Science*, the IEEE *Transactions on Geoscience and Remote Sensing* (TGRS), and the AMS *Journal of Atmospheric and Oceanic Technology*. He is currently the Editor-in-Chief of TGRS. He has been the recipient of three NASA Certificates of Recognition and four NASA Group Achievement Awards, as well as the 1997 TGRS Prize Paper Award, the 1999 IEEE Resnik Technical Field Award, and the 2006 International Geoscience and Remote Sensing Symposium Prize Paper Award.

Sidharth Misra received the B.E. degree in electronics and communication engineering from the Nirma Institute of Technology, Gujarat University, Ahmedabad, Gujarat, India, in 2004 and the M.S. degree in electrical engineering and computer science—signal processing from the University of Michigan, Ann Arbor, in 2006. He is currently working toward the Ph.D. degree in the Department of Atmospheric, Oceanic and Space Sciences, University of Michigan.

He was a Research Engineer with the Space Physics Research Laboratory, University of Michigan, where he worked on the analysis and implementation of the agile digital receiver for RFI mitigation. He was also on Oceansat-II with the Space Applications Center, Indian Space Research Organization, Ahmedabad. He was a Research Assistant with the Danish National Space Center, Technical University of Denmark (DTU), Lyngby, performing RFI analysis for CoSMOS, which is an airborne campaign preparing for SMOS at DTU. His research interests involve microwave radiometry, signal detection and estimation, and image processing.

Mr. Misra is the recipient of the IGARSS 2006 Symposium Prize Paper Award and first prize at the IGARSS 2009 student prize paper competition.

Simon H. Yueh (M'92–SM'01–F'09) received the Ph.D. degree in electrical engineering from the Massachusetts Institute of Technology, Cambridge, in January 1991.

He was a postdoctoral research associate at the Massachusetts Institute of Technology from February to August 1991. In September 1991, he was with the Radar Science and Engineering Section at the Jet Propulsion Laboratory (JPL), Pasadena, CA. He was the supervisor of radar system engineering and algorithm development group from 2002-2007. He became the deputy manager of Climate, Oceans and Solid Earth section in July 2007, and was promoted to the section manager in March 2009. He is also serving as the instrument scientist for the National Aeronautics and Space Administration (NASA) Aquarius mission for global sea surface salinity observations. He has been the Principal/Co-Investigator of numerous research projects, including the polarimetric wind radiometer research; airborne scatterometer project for hurricane wind measurements; Passive/Active L-band Sensor (PALS) project; NASA Instrument Incubator Project for a mission concept using a large mesh-deployable antenna for soil moisture and ocean salinity sensing; the airborne polarimetric radar (POLSCAT) for ocean wind velocity measurements; the POLSCAT/Cold Land Processes Experiments (CLPX-1 and -2) in 2002–2004 and 2006–2008; the Advanced Component Technology lightweight dual-frequency antenna feed project; the Aquarius PALS High Wind Campaign in 2009; the POLSCAT-CLPX3 experiment in 2009-2010. He is leading the development of Snow and Cold Land Processes mission concept at JPL. He has authored four book chapters and published more than 150 publications and presentations.

Dr. Yueh received the 2010 IEEE TGRS Transaction Prize Paper Award, 2003 IEEE GRSS Transaction Prize Paper award, the 2000 Best Paper Award in the IEEE International Geoscience and Remote Symposium 2000, and the 1995 IEEE GRSS Transaction Prize Paper award for a paper on polarimetric radiometry. He received the JPL Lew Allen Award in 1998 and Ed Stone Award in 2003. He is an associate editor of IEEE Transactions on Geoscience and Remote Sensing and is the Fellow of IEEE.

Steve J. DiNardo (M'95) received the B.S. degree from CSULA. In 1978, joined JPL's Section 335, he has been involved in various projects, including very long base interferometry (VLBI), mobile VLBI, experimental orbiting VLBI using the NASA TDRSS spacecraft, Water Vapor Radiometers, Topex Cal/Val, GPS receiver development and group leader of international GPS service.

In, 1995, Steve transferred to section 386, from 1995 through 1997, he was responsible for the deployment of the JPL aircraft polarimetric wind radiometers (WINDRAD) on NASA's DC-8 and P-3 and the Airborne Cloud Radar (ACR) on the DC-8. In 1998, He successfully coordinated the Hurricane Ocean Wind Experiment, sponsored by NASA and NPOESS, resulting in the first airborne Ku- Band scatterometer and multifrequecy polarimetric radiometers flights over hurricanes, for this effort, he received the NASA Exceptional Technical leadership award. He has also been responsible for development and deployment of JPL's aircraft rain radar and a 94-Ghz cloud profiling radar on NASA's DC-8. He built the JPL Ku-band polarimetric scatterometer (POLSCAT), deployed on the NCAR C-130, for the first successful demonstration of polarimetric wind scatterometer technique. He has been responsible for the deployment of POLSCAT and WINDRAD on the DC-8 to support the NASA Cold Land Process Experiment in 2002-2003. In 2004, built the GeoStar Geosynchronous microwave sounding instrument. In 2006, Steve managed the TWP-ICE experiment, using the Airborne Cloud Radar this time in a Twin Otter aircraft. In 2007 and 2008, supported NASA Cold Land Process Experiment flying POLSCAT over the North Slope of Alaska also in the Twin Otter. Also, in 2007, Steve supported and co-managed the CLASIC-07 experiment with 16 aircraft in Oklahoma. In 2009, Steve managed the PALS high wind mission using the P-3B flying in the Labrador Sea. He is involved in the development of low noise microwave radiometers and radar systems for aircraft and spacecraft for remote sensing of soil moisture and ocean salinity (PALS) in support of Aquarius, and SMAP. Steve is currently the NASA EV-1 CARVE Project Manager. Steve has received numerous NASA group achievement awards and has a US patent and is a member of the IEE.